PNAS PLUS

Unreplicated DNA remaining from unperturbed S phases passes through mitosis for resolution in daughter cells

Alberto Moreno[a,1], Jamie T. Carrington[a,1], Luca Albergante[a,b], Mohammed Al Mamun[a,b], Emma J. Haagensen[a,2], Eirini-Stavroula Komseli[c], Vassilis G. Gorgoulis[c,d,e], Timothy J. Newman[a,b], and J. Julian Blow[a,3]

[a]School of Life Sciences, University of Dundee, Dundee DD1 5EH, United Kingdom; [b]School of Science and Engineering, University of Dundee, Dundee DD1 4HN, United Kingdom; [c]Department of Histology and Embryology, School of Medicine, University of Athens, GR-11527 Athens, Greece; [d]Biomedical Research Foundation of the Academy of Athens, GR-11527 Athens, Greece; and [e]Faculty Institute of Cancer Sciences, Manchester Academic Health Science Centre, University of Manchester, Manchester M20 4QL, United Kingdom

Edited by James E. Cleaver, University of California, San Francisco, CA, and approved July 6, 2016 (received for review February 26, 2016)

To prevent rereplication of genomic segments, the eukaryotic cell cycle is divided into two nonoverlapping phases. During late mitosis and G1 replication origins are "licensed" by loading MCM2-7 double hexamers and during S phase licensed replication origins activate to initiate bidirectional replication forks. Replication forks can stall irreversibly, and if two converging forks stall with no intervening licensed origin—a "double fork stall" (DFS)—replication cannot be completed by conventional means. We previously showed how the distribution of replication origins in yeasts promotes complete genome replication even in the presence of irreversible fork stalling. This analysis predicts that DFSs are rare in yeasts but highly likely in large mammalian genomes. Here we show that complementary strand synthesis in early mitosis, ultrafine anaphase bridges, and G1-specific p53-binding protein 1 (53BP1) nuclear bodies provide a mechanism for resolving unreplicated DNA at DFSs in human cells. When origin number was experimentally altered, the number of these structures closely agreed with theoretical predictions of DFSs. The 53BP1 is preferentially bound to larger replicons, where the probability of DFSs is higher. Loss of 53BP1 caused hypersensitivity to licensing inhibition when replication origins were removed. These results provide a striking convergence of experimental and theoretical evidence that unreplicated DNA can pass through mitosis for resolution in the following cell cycle.

DNA replication | MCM | cell cycle | 53BP1 | UFB

During the eukaryotic cell cycle, the genome must be precisely duplicated with no sections left unreplicated and no sections replicated more than once. To prevent rereplication, the process is divided into two nonoverlapping phases: during late mitosis and G1 replication origins are "licensed" for subsequent use by loading MCM2-7 double hexamers, and during S phase DNA-bound MCM2-7 is activated to form processive CMG (CDC45-MCM-GINS) helicases that drive replication fork progression. The prohibition of origin licensing during S phase and G2 ensures that rereplication of DNA cannot occur. However, the inability to license new origins after the onset of S phase provides a challenge for the cell to fully replicate the genome using its finite supply of licensed origins. Replication forks can irreversibly stall when they encounter unusual structures on the DNA, such as DNA damage or tightly bound protein–DNA complexes.

When replication initiation occurs at a licensed replication origin the MCM2-7 double hexamer forms a pair of bidirectionally orientated CMG helicases (1–3). If one fork irreversibly stalls, the converging fork from a neighboring origin can compensate by replicating all of the DNA up to the stalled fork. However, if two converging forks both stall and there is no licensed origin between them—a "double fork stall" (DFS)—new replicative machinery cannot be recruited to replicate the intervening DNA (4). To compensate for this potential for underreplication, origins are licensed redundantly, with most (typically >70%) remaining dormant but capable of becoming active if necessary (5–9). We previously used mathematical analysis to show how the distribution of replication origins in yeasts can be explained by the need for complete genome replication in the presence of irreversible fork stalling (4). Our theory predicts that organisms with significantly larger genomes than yeast, such as those of mammals, will experience a much greater probability of replication failure genome-wide.

In this work, we provide evidence for a postreplicative mechanism that allows the resolution of these unreplicated segments of DNA that involves segregation of template DNA strands during mitosis by the creation of ultrafine anaphase bridges (UFBs) and their recognition in the subsequent G1 phase by the DNA repair protein p53-binding protein 1 (53BP1). We show that 53BP1 nuclear bodies correlate with the expected number of DFSs, both when the number of replication origins is reduced and when the number of replication origins is increased. We also show that 53BP1 preferentially associates with DNA in larger replicons, as predicted

Significance

We provide evidence that in organisms with gigabase-sized genomes, such as humans, one or more stretches of DNA typically remain unreplicated when cells enter mitosis and are segregated to daughter cells via structures called ultrafine anaphase bridges. p53-binding protein 1 (53BP1) accumulates at the subsequent DNA structures inherited by each daughter cell in the following G1 phase to facilitate resolution in S phase. We show that the abundance of these structures match theoretical predictions for the number of unreplicated DNA segments when the number of replication origins is artificially increased or decreased. We show that 53BP1 preferentially binds to chromosomal regions with low numbers of replication origins. This work challenges the prevailing view of how genome stability is maintained in proliferating cells.

Author contributions: A.M. designed, performed, and optimized experiments on 53BP1 nuclear bodies, UFBs and immunofluorescence, and ChIP-Seq; J.T.C. performed experiments on 53BP1 nuclear bodies, RPA and γ-H2AX foci, mitotic EdU, and clonogenic assays and performed the flow-cytometry experiments; L.A. performed the ChIP-Seq analysis; L.A. and M.A.M. performed the mathematical and computational analyses; A.M. and E.J.H. developed the 3D FACS protocol; E.-S.K. and V.G.G. made the HBEC cells; A.M. and J.T.C. analyzed data; T.J.N. coordinated the theoretical work; J.J.B. led the project; and A.M., J.T.C., and J.J.B. wrote the paper.

The authors declare no conflict of interest.

This article is a PNAS Direct Submission.

Freely available online through the PNAS open access option.

[1]A.M. and J.T.C. contributed equally to this work.

[2]Present address: Northern Institute for Cancer Research, Medical School, Newcastle University, Newcastle upon Tyne NE2 4HH, United Kingdom.

[3]To whom correspondence should be addressed. Email: j.j.blow@dundee.ac.uk.

This article contains supporting information online at www.pnas.org/lookup/suppl/doi:10.1073/pnas.1603252113/-/DCSupplemental.

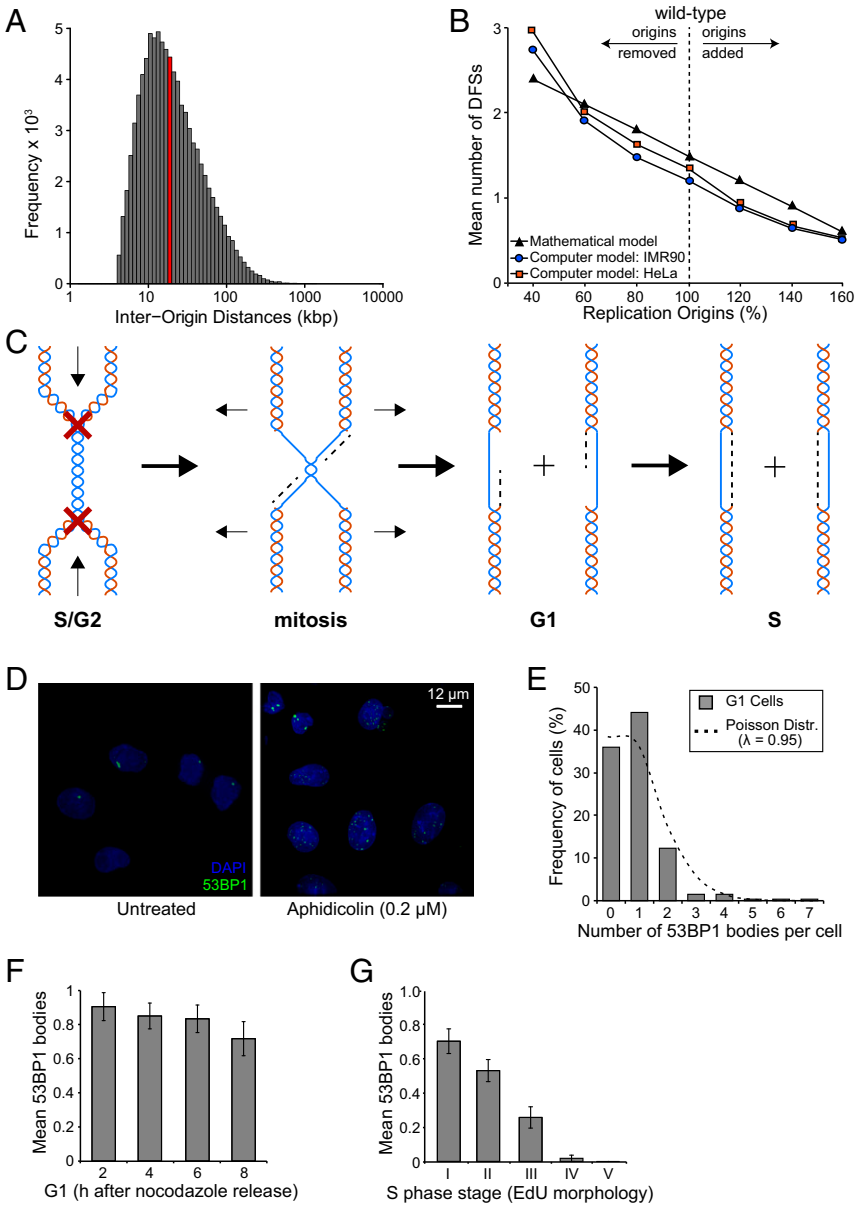

Fig. 1. Potential mechanism for resolution of DFSs. (*A*) Distribution of replicon sizes in HeLa cells, based on data from ref. 13. The red bar represents the average replicon size of ∼31 kb. (*B*) Mean number of DFSs predicted using a mathematical model (4), and a computational model that uses origin data from HeLa and IMR-90 (13) when origins are added or depleted randomly. (*C*) Model for segregation of unreplicated DNA to daughter cells for resolution in the next cell cycle. (*D*) The 53BP1 nuclear bodies in untreated and aphidicolin-treated cells. (*E*) Frequency of G1-specific 53BP1 nuclear bodies ($n = 100$, three replicates). χ^2 test for a fitted Poisson, $P = 0.771$. (*F*) Frequency of G1-specific 53BP1 nuclear bodies at the times indicated after nocodazole treatment and mitotic shake-off ($n = 150$, three replicates, error bars are SEM). χ^2 test, $P = 0.924$. (*G*) Frequency of 53BP1 nuclear bodies at different stages of the replication timing program, as defined by O'Keefe et al. (32) ($n = 150$, three replicates, error bars are SEM). χ^2 test, $P = 4.998 \times 10^{-4}$.

by the theoretical analysis. This experimental work strongly supports the theoretical analysis of DFSs in organisms of differing genome size that we present in an accompanying paper (10).

Results

Refinements in technology have led to a convergence of origin mapping data in mammalian tissue culture cells (11–13). Fig. 1*A* shows the spacing between ∼90,000 replication origins (i.e., the replicon sizes) in HeLa cells derived from the data of Picard et al. (13). The average interorigin distance is ∼31 kb, consistent with initiation events being ∼100 kb apart (11, 14, 15) and ∼30% of origins being stochastically activated in any given S phase (6–9, 16, 17). Compared with yeast, human cells have an irregular distribution of origins with an unexpectedly high number of very large replicons (10). Using a mathematical approach that we have previously derived and validated (4) we estimate that one or two DFSs are expected to occur in every HeLa cell S phase (Fig. 1*B*). Similar numbers were obtained when we performed computational analyses based on the origin mapping data from both HeLa and primary IMR90 cells (Fig. 1*B*). The predicted number of DFSs increases when replication origins are removed and decreases when they are added (Fig. 1*B*). Theoretical analysis indicates that the distribution of origins in human cells is constrained to produce, on average, only a small number of DFSs and therefore indicates that human cells should possess a postreplicative mechanism capable of resolving these spontaneous events (10).

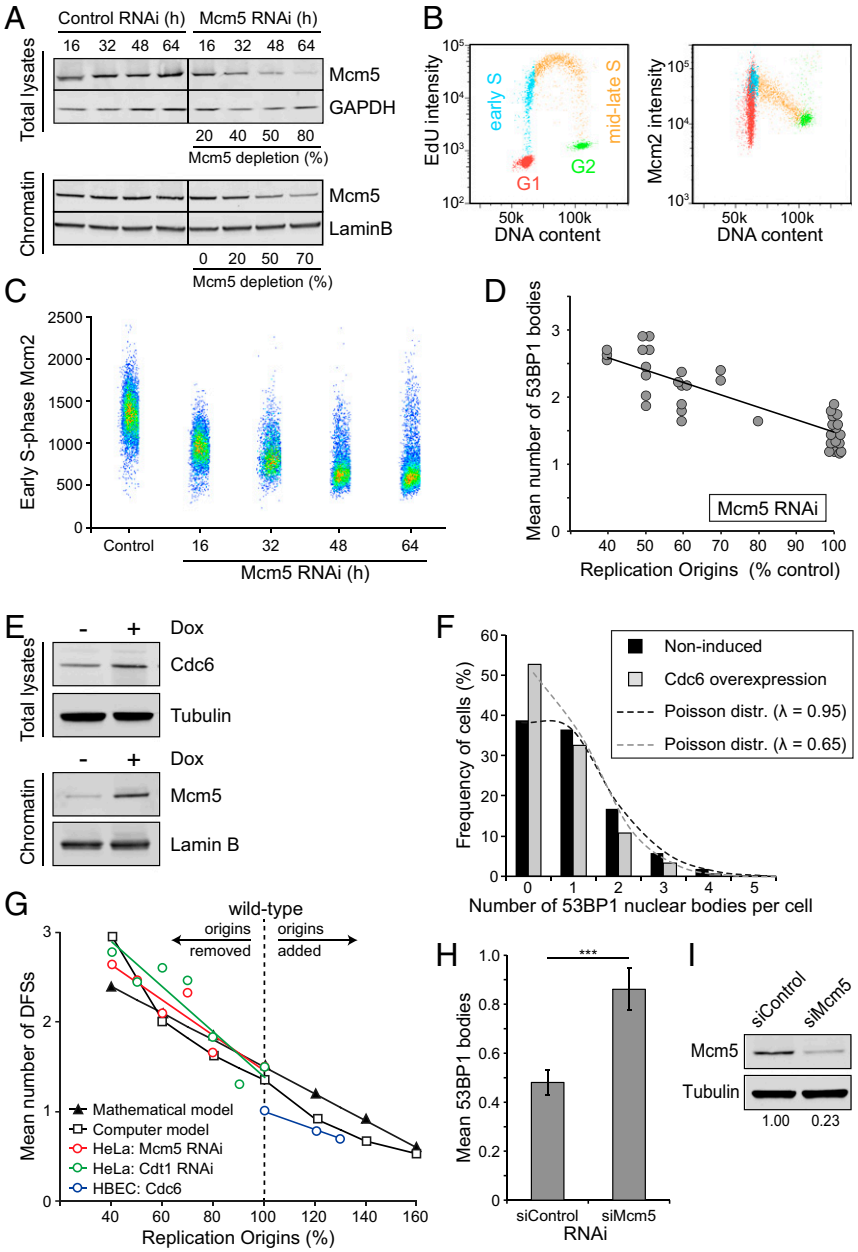

Fig. 2. Origin number and the frequency of 53BP1 nuclear bodies. (*A*) Immunoblot of total and chromatin-bound MCM5 in HeLa cells after MCM5 RNAi. (*B*) Three-dimensional FACS of HeLa cells labeled with EdU (*Left*) and MCM2 (*Right*). Red, G1 phase: EdU negative and G1 DNA content. Blue, early S phase: incorporation of EdU without significant increase in total DNA content. Orange, late S phase: EdU positive cells with >G1 DNA content. Green, G2 phase: EdU negative and G2 DNA content. (*C*) FACS of chromatin-associated MCM2 signal in early S phase HeLa cells with indicated periods of MCM5 RNAi. (*D*) Frequency of G1-specific 53BP1 nuclear bodies (*y*-axis values) after MCM5 knockdown versus relative number of replication origins quantified by 3D FACS of DNA-bound MCM2 (*x*-axis values). Each point represents the mean of 100 cells. (*E* and *F*) CDC6-inducible HBEC cells. Immunoblot of CDC6 and tubulin in whole-cell lysates (*E*, *Top*) and MCM5 and Lamin B1 in chromatin samples (*E*, *Bottom*). Frequency distribution of 53BP1 nuclear bodies in HBEC cells (*F*) ($n = 100$, three replicates). χ^2 tests for fitted Poissons, $P > 0.87$. The two conditions are significantly different (Wilcoxon rank sum test, $P = 2.843 \times 10^{-6}$). (*G*) Compilation of the predicted number of DFSs using the mathematical model and the computer simulation (from Fig. 1*B*) and the mean number of 53BP1 nuclear bodies in vivo (from *D* and *F* and Fig. S2*E*). (*H*) Frequency of G1-specific 53BP1 nuclear bodies in control and MCM5 RNAi-treated IMR-90 cells ($n = 150$, three replicates, error bars are SEM). *t* test, $P = 1.79 \times 10^{-4}$. (*I*) Immunoblot to show the depletion of MCM5 after RNAi. Quantification of band intensity is indicated below the blot.

Because a DFS will create a large segment of unreplicated DNA, our analyses suggest that humans and metazoans in general with significantly larger genomes than yeasts have evolved mechanisms to resolve them. Unreplicated or damaged DNA may require topological unhooking for accurate segregation during mitosis and the lesions generated by this process could then be repaired in the following cell cycle (18, 19) (Fig. 1*C*). Chromatid condensation during mitosis could provide a processive unwinding activity to separate unreplicated DNA, leaving single-stranded gaps that could then be partially filled in during mitosis (20) or the following cell cycle. This mechanism depends on the resolution and segregation of topologically intertwined strands and could require a limited amount of DNA strand cutting (19–21). We therefore predict that this mechanism might be able to deal with only a small number of DFSs, as our theory predicts (10).

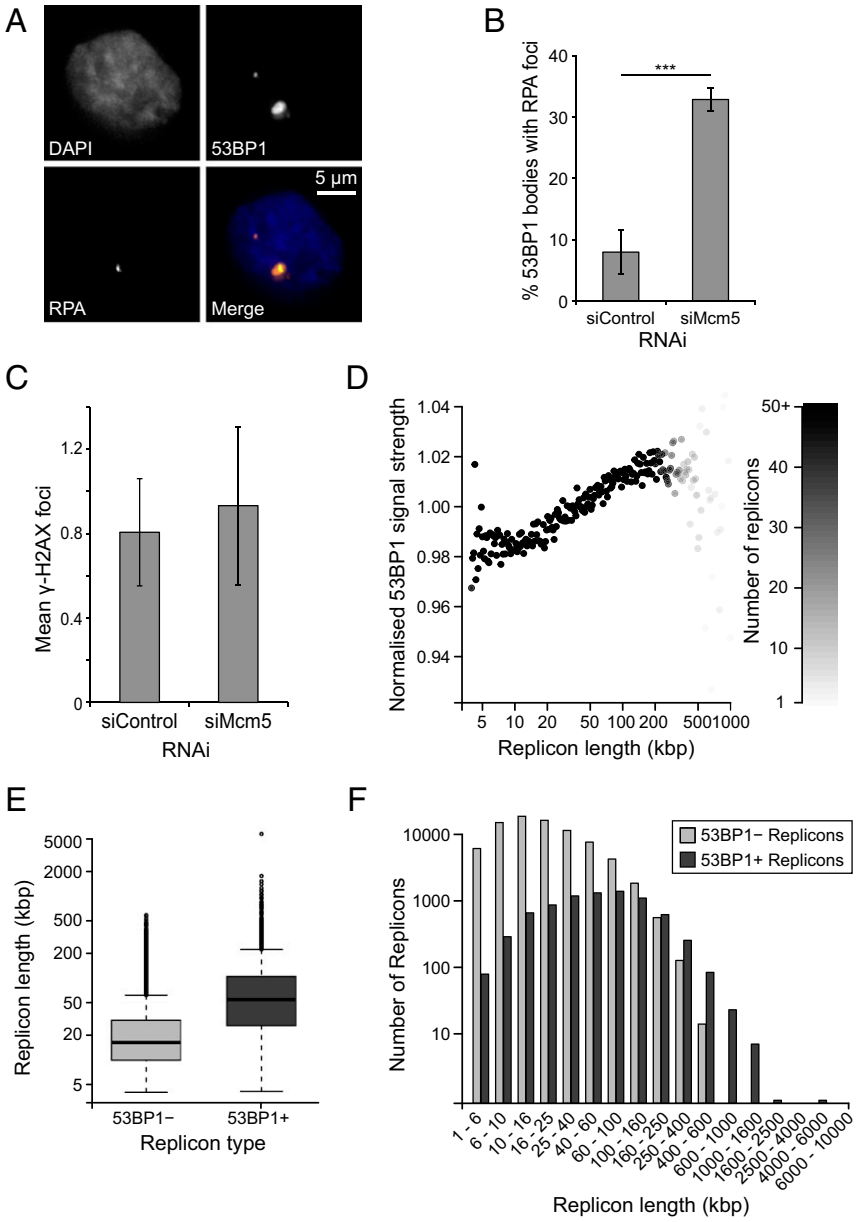

Fig. 3. The 53BP1 is enriched at genomic loci that correspond to large replicons. (*A*) Representative image of the colocalization between G1-specific 53BP1 nuclear bodies and RPA foci. (*B*) Percentage of total cellular 53BP1 nuclear bodies that colocalize with RPA after treatment with control or MCM5 RNAi (n = 100, three replicates, error bars are SEM). t test, $P = 3.01 \times 10^{-3}$. (*C*) Mean frequency of G1-specific γ-H2AX foci in HeLa cells after MCM5 RNAi (n = 150, three replicates, error bars are SEM). t test, $P = 0.585$. (*D*) Plot of the average 53BP1/IgG signal ratio per kilobase against replicon size. A strong and significant correlation is observed (Spearman $\rho = 0.91$, $P < 10^{-15}$). (*E*) Distribution of the size of 53BP1+ and 53BP1− replicons. t test, $P < 10^{-15}$. (*F*) Frequency distribution of 53BP1+ and 53BP1− replicons across different replicon sizes. χ^2 test, $P < 10^{-15}$.

Previous studies have suggested that 53BP1 recognizes these aberrant structures in the cell cycle following underreplication. The 53BP1 forms "nuclear bodies" in G1 phase that are symmetrically distributed between sister cells, possibly corresponding to lesions generated by transmission of DFSs through mitosis in the parent cell (18, 22). Consistent with this idea, the number of 53BP1 nuclear bodies increases in cells treated with replication inhibitors (23–25) (Fig. 1*D* and Fig. S1 *A* and *B*), suggesting that 53BP1 can recognize structures resulting from defective DNA replication. As our theory predicts (10), 53BP1 nuclear bodies in normal G1 phase HeLa cells conform to a Poisson distribution (suggesting that they are due to independent stochastic events) with a mean close to the predicted number of DFSs (Fig. 1*E* and Fig. S1 *C* and *D*). The number remains stable during G1 (Fig. 1*F*) but declines as cells progress through S phase, supporting the idea that they are resolved in a replication-dependent manner (Fig. 1*G* and Fig. S1*E*).

To provide evidence for a link between DFSs and 53BP1 nuclear bodies, we depleted replication origins in HeLa cells using RNAi against two components of the origin licensing system, MCM5 and CDT1 (6) (Fig. 2*A* and Fig. S2*A*). We then used a 3D flow cytometry protocol, measuring DNA content, 5-ethynyl-2′-deoxyuridine (EdU) incorporation, and chromatin-bound MCM2 to determine the amount of chromatin-bound MCM2-7 in cells entering S phase (Fig. 2*B*). Because origins are only licensed for use if they are associated with MCM2-7, the amount of DNA-bound MCM2 at the onset of S phase provides a measure of the number of available origins. Depletion of MCM5 by RNAi

reduced the amount of DNA-bound MCM2 at S phase entry (Fig. 2*C*). Similar results were obtained with RNAi against the licensing factor CDT1 (Fig. S2 *A* and *B*). In both cases, overall EdU incorporation was not affected (Fig. S2*C*). In line with our theoretical predictions, the number of 53BP1 nuclear bodies increased in proportion to the reduction in DNA-bound MCM2 (Fig. 2*D* and Fig. S2 *D* and *E*). Similar results were obtained in U2OS cells treated with MCM5 RNAi (Fig. S2 *F* and *G*).

Our theory also predicts that if cells have higher than normal numbers of licensed origins, the number of DFSs should reduce (Fig. 1*B*). To increase DNA-bound MCM2-7 we used a human bronchial epithelial cell line overexpressing the licensing protein CDC6 (Fig. 2*E*). The number of 53BP1 nuclear bodies in these hyperlicensed cells was reduced 30% compared with noninduced controls (Fig. 2*F* and Fig. S3 *A* and *B*), in line with our model. Fig. 2*G* combines all our data on the number of 53BP1 nuclear bodies (Fig. 2 *D* and *F* and Fig. S2*E*) to show that there is excellent agreement between our theoretical predictions (Fig. 1*B*) and the experimental data from cells with reduced or increased numbers of licensed origins. Fig. 2 *H* and *I* shows that there is also an increase in the frequency of 53BP1 nuclear bodies after MCM5 RNAi treatment of primary IMR-90 cells. This suggests a similar relationship between the amount of DNA-bound MCM2-7 and the number of 53BP1 nuclear bodies in both normal cells (IMR-90) and cancer cells (HeLa and U2OS). Taken together, our data provide strong support for the idea that failures of DNA replication caused by spontaneous DFSs cause the appearance of 53BP1 nuclear bodies in the subsequent G1.

We next investigated the nature of the lesions marked by 53BP1 nuclear bodies in G1 cells. Our theory suggests that these structures represent single-stranded or partially single-stranded regions of DNA rather than double-strand DNA breaks (Fig. 1*C*). We therefore investigated the colocalization of 53BP1 nuclear bodies with the ssDNA binding protein RPA (replication protein A). Fig. 3 *A* and *B* shows that in untreated cells ∼7% 53BP1 nuclear bodies were associated with measurable levels of RPA (18), but partial depletion of MCM2-7 caused a large increase in colocalization to >30%. The increase of RPA in 53BP1 nuclear bodies in cells with a reduced origin number might reflect the larger distance between stalled forks, and hence longer stretches of unreplicated DNA that bind RPA. To rule out the possibility that G1-specific 53BP1 nuclear bodies mark double-strand breaks generated by synthetic reduction of licensed origins in the preceding S phase, we also quantified the frequency of G1-specifc γ-H2AX foci in response to MCM5 RNAi (Fig. 3*C* and Fig. S4). No significant increase of G1-specifc γ-H2AX foci was observed between the control and cells depleted of MCM5 (*t* test, $P = 0.59$).

Although DFSs can occur at any region of the genome, theoretical analysis predicts that they are more likely in larger replicons rather than in smaller ones (4). To test this, we performed chromatin immunoprecipitation with anti-53BP1 antibodies and sequenced the precipitated DNA (Fig. S5). Cell fractionation and immunoblotting revealed that a majority of 53BP1 (∼75%) is associated with chromatin (Fig. S6*B*), and quantification of GFP-53BP1 intensity revealed that only ∼1% of 53BP1 signal originates from nuclear bodies (Fig. S6*A*). This means that the majority of DNA bound by 53BP1 is not associated with 53BP1 nuclear bodies. Consistent with this, the total genomic coverage from 53BP1 and IgG precipitations were comparable (Fig. S6*C*). However, the 53BP1/IgG binding ratio showed a highly significant correlation between replicon size and the strength of 53BP1 association (Fig. 3*D* and Fig. S5*D*). We then identified 1-kb regions of the genome with a high 53BP1/IgG ratio ($P < 10^{-3}$); replicons were defined as 53BP1+ when they contained one or more 53BP1-enriched regions and 53BP1− otherwise. 53BP1+ replicons were on average approximately three times larger than 53BP1− replicons (Fig. 3 *D* and *E* and Fig. S6*F*). There was also a weak correlation between 53BP1 binding, chromosome fragile sites, and late-replicating DNA (Fig. S6 *D* and *E*). Taken together, these analyses show that 53BP1 is more likely to bind to DNA in large replicons, as predicted if 53BP1 recognizes DNA structures resulting from DFSs.

The recent discovery that aphidicolin-treated cells exhibit EdU incorporation during early mitosis indicates that replication stress causes damage that is resolved postreplicatively by DNA repair synthesis (20). If unreplicated DNA is unwound during mitosis, ssDNA will be exposed, thereby providing a template for complementary strand synthesis. Consistent with this idea, MCM5 RNAi caused a significant increase in early-mitotic EdU foci (Fig. 4 *A*–*C*). This result, when combined with the colocalization of 53BP1 and RPA and lack of increased γ-H2AX foci (Fig. 3*A*), implies that the foci of EdU incorporation during early mitosis represent sites of DNA synthesis of unreplicated DNA (dashed lines in Fig. 1*C*).

This postreplicative mechanism may not be able to complete replication of all of the unreplicated DNA generated by DFSs, which may be hundreds of kilobases in size (10). It has been suggested that UFBs, which contain single-stranded DNA, might represent a mechanism for resolving partially replicated stretches of DNA (20, 26–29) (dashed lines in Fig. 1*C*). Consistent with this idea, we observed that in untreated HeLa cells the number and distribution of UFBs closely matched the numbers of 53BP1 nuclear bodies. Further, the number of UFBs increased in line with 53BP1 nuclear bodies when MCM2-7 was partially depleted. This is consistent with the idea that UFBs provide a mechanism by which unreplicated DNA generated by DFSs is transmitted through mitosis to daughter cells to become ssDNA lesions coated with 53BP1 that form nuclear bodies (Fig. 4 *D*–*F*).

Because we predict that DFSs occur frequently in normal cells, 53BP1 is likely to be performing a function in binding to the products of DFSs in G1 phase. The 53BP1 is known to protect damaged DNA from undergoing homologous recombination (30) and could perform this function at DFSs, which may allow the structures to be resolved by an alternative pathway in S phase. To explore this idea further, we examined a possible synthetic interaction between loss of 53BP1 and an increase in DFSs created by partial knockdown of MCM2-7. RNAi transfected cells were treated with increasing concentrations of hydroxyurea (HU) before a colony assay was performed. Cells partially depleted for MCM2-7 were hypersensitive to HU, due to their inability to use dormant replication origins (6–8). The 53BP1-depleted cells showed a sensitivity similar to that of control cells. However, cells depleted of 53BP1 showed a highly synergistic sensitivity to HU when combined with partial knockdown of MCM5 (Fig. 4 *G* and *H* and Fig. S6*G*). This shows that although 53BP1 is not essential it works together with dormant origins to protect cells from the consequences of replication fork failure.

Discussion

In this work we present evidence that in unperturbed cell cycles of human cells unreplicated DNA is frequently present at the end of G2, is partially filled in during early mitosis, and is segregated during mitosis for resolution during the following cell cycle. Our theoretical analysis (4, 10) suggests that in organisms such as humans with gigabase-sized genomes DFSs will routinely occur and create sections of unreplicated DNA that must be resolved by a postreplicative mechanism. The symmetrical distribution of 53BP1 nuclear bodies between daughter cells and their induction by replicative stresses means that they could mark the products of unreplicated DNA segregated to daughter cells. We show that when replication origins are deleted or added there is a strong correlation between the number of 53BP1 nuclear bodies and our theoretical predictions of DFSs as presented in our accompanying paper (10). We show that 53BP1 preferentially associates with larger replicons, in line with our theoretical predictions of DFS distribution. We also provide evidence for a mechanism for the processing of the unreplicated

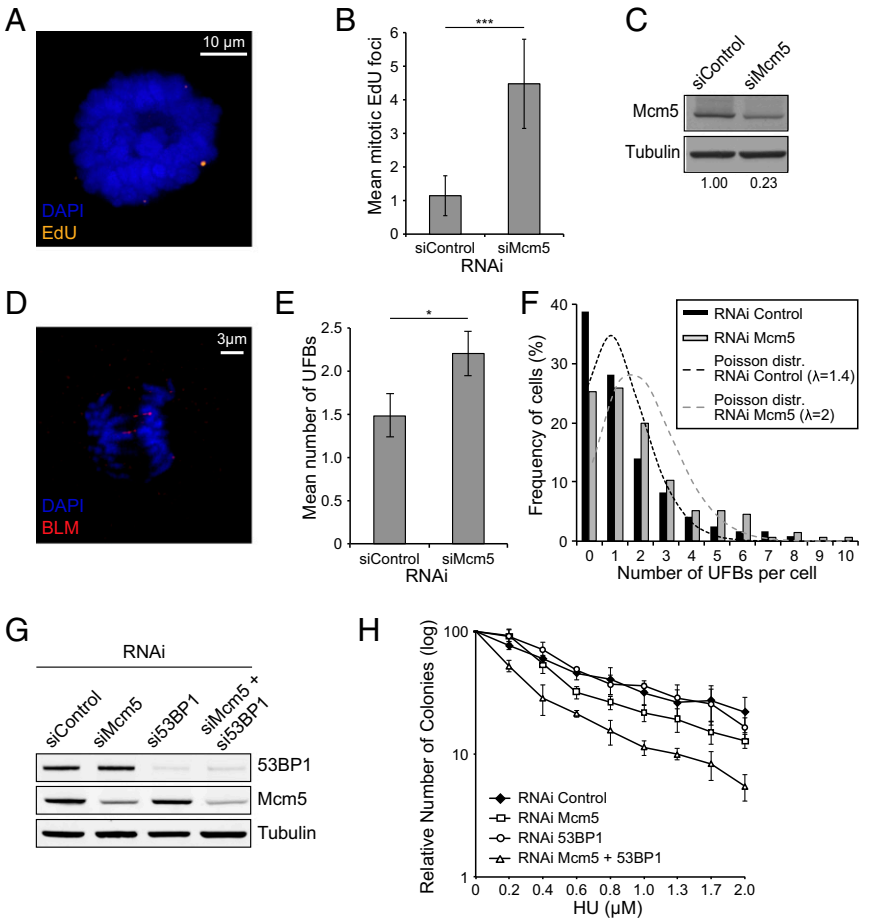

Fig. 4. MCM5 RNAi effects on mitosis. (*A*) Representative image of early-mitotic HeLa cell with foci of EdU incorporation. (*B*) Quantification of foci of EdU incorporation during prophase and prometaphase HeLa cells after MCM5 RNAi (n = 100, three replicates, error bars are SEM). t test, $P = 3.43 \times 10^{-8}$. (*C*) Immunoblot to show depletion of MCM5 after MCM5 RNAi. Quantification of band intensity is indicated below the blot. (*D*) Representative image of UFBs stained with BLM in an anaphase HeLa cell. (*E*) Frequency of UFBs after 48-h treatment with MCM5 RNAi (n = 75, three replicates, error bars are SEM). t test, $P = 0.0473$. (*F*) Frequency distribution of UFBs (n = 100 cells, four replicates). χ^2 tests for Poissons, $P > 0.85$. A significant difference was observed. Wilcoxon rank sum test, $P = 5.095 \times 10^{-3}$. (*G*) Immunoblot showing the knockdown of MCM5 and 53BP1 by RNAi in HeLa cells. (*H*) Clonogenic assay after treatment, as seen in *G*, with increasing HU (three replicates, error bars are SEM).

DNA between DFSs, involving complementary strand synthesis occurring in early mitosis, the resolution of partially replicated DNA via UFBs, and their association with 53BP1 in G1.

A recent paper has shown that when DNA replication is inhibited the condensation of chromosomes during early mitosis is associated with the appearance of focal sites of DNA synthesis (20). Our theoretical work is based on the idea that, from the end of G1 through to the end of metaphase, MCM2-7 cannot be loaded onto DNA even if DFSs have occurred (4, 10). MCM2-7 forms the core of the replicative CMG helicase that unwinds DNA at the replication fork, and so the essential problem for completing replication at DFSs is to provide an alternative DNA unwinding activity. The chromosome condensation that resolves sister chromatids during early mitosis could provide such an alternative DNA unwinding activity. Once ssDNA is exposed, DNA polymerases will perform complementary strand synthesis to substantially fill in the gaps. Consistent with this we show that the frequency of foci of DNA synthesis in early mitosis is in line with our predictions of the number of DFSs and increases when origin number is reduced.

We imagine that this complementary strand synthesis, which is not driven by a processive helicase, might not always fully complete DNA replication but may leave small gaps or lesions on the DNA. UFBs represent a potential intermediate that could allow such partially unreplicated DNA segments arising from DFSs to be segregated to daughter cells (18–20). We show that the number of UFBs in untreated cells increases in line with our predictions when origin number is reduced.

Consistent with our theoretical model, we show that 53BP1 is preferentially bound to DNA in larger replicons, where DFSs are more likely to occur. Under normal circumstances, there is only a low colocalization of RPA with 53BP1 nuclear bodies, but this increases markedly when origin number is reduced. We imagine that normally a significant proportion of the remaining unreplicated DNA can undergo complementary strand synthesis in early mitosis, leaving little ssDNA to bind RPA in the subsequent G1. However, the distance between stalled forks in DFSs will increase following a reduction in origin number, and this should result in more ssDNA remaining after progression through mitosis, as we demonstrate. We also show that the increase in 53BP1 nuclear bodies in G1 is not significantly associated with an increase of γ-H2AX foci after partial depletion of origins, suggesting that 53BP1 nuclear bodies are not simply sites of double-stranded DNA breaks. The 53BP1 nuclear bodies are ultimately dispersed as the DNA replicates during S phase, suggesting that the unusual DNA structures that they mark are not fully resolved until another round of replication has occurred.

Finally, we show that 53BP1 synergizes with dormant origins to protect genome integrity in the presence of replicative stress, as evidenced by its hypersensitivity to HU when the number of

dormant origins was reduced. The 53BP1 gene (TP53BP1) is not essential and has been associated with protecting damaged DNA from undergoing inappropriate homologous recombination (30). The synthetic interaction that we show between loss of 53BP1 and partial MCM knockdown could therefore be a consequence of unreplicated DNA undergoing inappropriate homologous recombination during S phase.

In the accompanying paper (10) we provide a theoretical analysis of origin distribution that leads to the conclusion that DFSs are almost inevitable in the large genomes of human cells. The experimental work presented here provides a potential mechanism by which DFSs can be processed, involving partial filling-in of unreplicated segments during early mitosis, segregation to daughter cells via UFBs, their association with 53BP1 nuclear bodies during G1, and their ultimate resolution during the next S phase. Our work therefore provides both experimental and theoretical evidence that structures resulting from replication failure can pass through mitosis for resolution in the next cell cycle.

Materials and Methods

Cell Culture. HeLa and IMR-90 cells were obtained from the American Type Culture Collection and used at a population doubling level lower than 30 and 20, respectively, and maintained in DMEM (41966; Invitrogen), supplemented with 10% FBS (10270106; Invitrogen) and penicillin and streptomycin at 37 °C in 5% CO_2. HBEC-Cdc6-Tet-On (human bronchial epithelial cells) were grown in keratinocyte serum-free medium (17005-075; Invitrogen) supplemented with 50 μg/mL bovine pituitary extract and 5 ng/mL hEGF (17005-075; Invitrogen). The HBEC cell line was developed as described in ref. 31. Briefly, immortalized HBECs were infected with PLVX-Tet-On with blasticidin resistance (3 μg/mL) and PLVX-TRE-Cdc6 with zeocin resistance (12.5 μg/mL). Clones with robust doxycycline-dependent induction (5 μg/mL) were selected.

RNAi and Transfections. siRNA duplexes were obtained from Thermo Fisher Scientific, and the sequences were as follows: control: 5′-UAGCGACUAAACACAUCAA -3′; MCM5: 5′-GGAUCUGGCCAGCUUUGAU -3′; CDT1: SMARTPool M-003248-02; and 53BP1: 5′- GAAGGACGGAGUACUAAUA-3′.

Transfection was performed with Lipofectamine RNAiMAX (Invitrogen). Fifty nanomolar siRNA was mixed with the Lipofectamine in Opti-MEM medium (Invitrogen). The mixture was added to 50–60% confluent cells in antibiotic-free DMEM (Invitrogen). Cells were subjected to different times of transfection to obtain variable reductions in protein level.

Immunoblotting and Antibodies. Immunoblotting was performed as previously described (8). Western blotting was performed according to standard procedures. Extraction of the chromatin-bound fraction was performed by treatment with CSK extraction buffer (10 mM Hepes, pH 7.4, 300 mM sucrose, 100 mM NaCl, 3 mM $MgCl_2$, and 0.5% Triton-X-100) for 10 min on ice. The pellet, containing chromatin-associated proteins, was processed for Western blotting. The antibodies used were MCM5 (sc-136366; Santa Cruz), CDT1 (ab183478; Abcam), tubulin (T6199; Sigma-Aldrich), 53BP1 (A300-272A; Bethyl), Lamin B1 (16048; Abcam), GAPDH (ab9484; Abcam), and CDC6 (05-550; Millipore).

Immunofluorescence. Cells were seeded in six-well plates containing glass coverslips. At the required times for each experiment they were fixed with 4% (vol/vol) formaldehyde, permeabilized with 0.1% Triton X-100 in TBS, and blocked with 0.5% fish skin gelatin (G-7765; Sigma) for 1 h. Cells were then incubated with the relevant antibodies overnight at 4 °C and washed with 0.1% TBS-Tween before incubation with Alexa secondary antibodies (Invitrogen). Cells were incubated with DAPI (D9542; Sigma) and mounted using Vectashield mounting medium (H-1000; Vector Laboratories). The antibodies used were 53BP1 (NB-100-904; Novus), Cyclin A (ab16726; Abcam), BLM (sc-7790; Santa Cruz), RPA (ab2175; Abcam), γ-H2AX (2577L; Cell Signaling), and phospho-histone H3 (9701S; Cell Signaling). For incorporation of EdU during early mitosis, asynchronous HeLa cells were incubated in 40 μM EdU (Invitrogen) for 30 min before fixation. To visualize incorporated EdU the cells were incubated in Click-iT EdU reaction, following the manufacturer's protocol (Thermo Fisher Scientific). Cells in prophase and prometaphase were identified by phospho-H3 antibody signal and DAPI morphology.

Image Acquisition and Analysis. Microscopy images were acquired using an Olympus IX70 deltavision deconvolution microscope. An Olympus 63× oil immersion objective was used, and images were captured using a CCD camera. Data from microscopy experiments was analyzed using Volocity 3D analysis software (PerkinElmer). The nucleus was outlined as the region of interest, and lower intensity threshold was set to a number that indicated the intranuclear background.

Three-Dimensional Flow Cytometry. Cells were incubated with 40 μM EdU (Invitrogen) for 30 min before trypsinization and collection. Cells were preextracted with CSK extraction buffer for 10 min on ice and then fixed in 2% (vol/vol) formaldehyde for 15 min. For MCM2 labeling, cells were permeabilized in ice-cold 70% (vol/vol) ethanol for 10 min and incubated for 1 h with anti-BM28 primary antibody (1:500). After staining with AlexaFluor 488-labeled secondary antibody (Invitrogen) cells were washed and Click-it EdU reaction was performed for 30 min. Finally, cells were treated with propidium iodide (PI) solution (50 μg/mL PI, 50 μg/mL RNaseA, and 0.1% Triton-X-100) and transferred to FACS tubes for analysis. Samples were acquired using a BD FACSCanto and the results analyzed using FlowJo software.

ChIP Sequencing. Cells were cross-linked for 30 min using 1.5 mM ethylene glycol-bis(succinimidyl succinate) followed by 10 min with 1% formaldehyde. Reactions were stopped with 2 M glycine and cells were resuspended in CSK buffer for 10 min. Cells were treated with 5 μL micrococcal nuclease (2,000 U/μL) for 10 min at 37 °C, neutralized with 2× RIPA [100 mM Tris·HCl, pH 7.4, 300 mM NaCl, 2% (vol/vol) IGE-Pal CA-630, 0.5% Na deoxycholate, and 1 mM EDTA] and incubated on ice for 10 min. Samples were then precleared with Protein A Dynabeads for 1 h at 4 °C and then incubated with 7 μg anti-53BP1 antibody (A300-272A; Bethyl) rotating overnight at 4 °C. DNA was eluted (1% SDS, 0.1 M $NaHCO_3$, and 0.1% Tween-20) and used for library preparation using the NEBNext ChIP-seq kit and sequenced on an Illumina HiSEq 2500 by Edinburgh Genomics. The raw sequence data were assessed, aligned, and combined using R version 3.2.2, Rsubread version 1.20.2, and SAMtools version 1.2. Aligned reads were analyzed using a script based on R version 3.2.2 and Rsamtools 1.22. The quality assessment and a detailed description of the analysis pipeline are available in *SI Materials and Methods*. Files containing the aligned reads are available at the European Nucleotide Archive (accession no. PRJEB12222) and the R script used for the analysis is available as Dataset S1.

Mathematical and Computational Analysis. The mean number of DFSs was computed with the formula

$$\log(2)\frac{N_g}{N_s} - \sum_{i=1}^{K} \log\left(1 + \log(2)\frac{N_i}{N_s}\right),$$

where N_g indicates the genome size, N_S indicates the median stalling distance, and the $N_i (i = 1..k)$ indicate the length of the K replicons. Replication origin (RO) depletion and augmentation experiments were performed by randomly removing or increasing the number of ROs. More details on the mathematical model used are described in refs. 4 and 10 and an extended summary of the approach used is available in *SI Materials and Methods*.

Clonogenic Assay. Cells were transfected in 10-cm dishes and replated into six-well dishes before treatment. HU was added to cells for 48 h before medium was replaced with fresh growth medium. After 10 d, cells were washed, fixed, and stained with Crystal Violet. The number of colonies >1 mm were recorded. For each genotype, cell viability of untreated cells was defined as 100%.

ACKNOWLEDGMENTS. This work was supported by Wellcome Trust Grants WT096598MA and 097945/B/11/Z; Greek General Secretariat for Research and Technology Program of Excellence II (Aristeia II) Grant 3020 (to V.G.G.); the Dundee Imaging Facility, supported by Wellcome Trust Award 097945/B/11/Z and Medical Research Council Award MR/K015869/1; and the Flow Cytometry and Cell Sorting Facility at the University of Dundee. V.G.G. and E.-S.K. received an Experimental Research Center Elpen Scholarship and National Scholarships Foundation-Siemens Aristeia Fellowship.

1. Evrin C, et al. (2009) A double-hexameric MCM2-7 complex is loaded onto origin DNA during licensing of eukaryotic DNA replication. *Proc Natl Acad Sci USA* 106(48): 20240–20245.
2. Gambus A, Khoudoli GA, Jones RC, Blow JJ (2011) MCM2-7 form double hexamers at licensed origins in Xenopus egg extract. *J Biol Chem* 286(13):11855–11864.
3. Remus D, et al. (2009) Concerted loading of Mcm2-7 double hexamers around DNA during DNA replication origin licensing. *Cell* 139(4):719–730.
4. Newman TJ, Mamun MA, Nieduszynski CA, Blow JJ (2013) Replisome stall events have shaped the distribution of replication origins in the genomes of yeasts. *Nucleic Acids Res* 41(21):9705–9718.

5. Woodward AM, et al. (2006) Excess Mcm2-7 license dormant origins of replication that can be used under conditions of replicative stress. *J Cell Biol* 173(5):673–683.
6. Ge XQ, Jackson DA, Blow JJ (2007) Dormant origins licensed by excess Mcm2-7 are required for human cells to survive replicative stress. *Genes Dev* 21(24):3331–3341.
7. Ibarra A, Schwob E, Méndez J (2008) Excess MCM proteins protect human cells from replicative stress by licensing backup origins of replication. *Proc Natl Acad Sci USA* 105(26):8956–8961.
8. Ge XQ, Blow JJ (2010) Chk1 inhibits replication factory activation but allows dormant origin firing in existing factories. *J Cell Biol* 191(7):1285–1297.
9. Blow JJ, Ge XQ, Jackson DA (2011) How dormant origins promote complete genome replication. *Trends Biochem Sci* 36(8):405–414.
10. Mamun AM, et al. (2016) Inevitability and containment of replication errors for eukaryotic genome lengths spanning megabase to gigabase. *Proc Natl Acad Sci USA* 113:E5765–5774.
11. Besnard E, et al. (2012) Unraveling cell type-specific and reprogrammable human replication origin signatures associated with G-quadruplex consensus motifs. *Nat Struct Mol Biol* 19(8):837–844.
12. Mesner LD, et al. (2013) Bubble-seq analysis of the human genome reveals distinct chromatin-mediated mechanisms for regulating early- and late-firing origins. *Genome Res* 23(11):1774–1788.
13. Picard F, et al. (2014) The spatiotemporal program of DNA replication is associated with specific combinations of chromatin marks in human cells. *PLoS Genet* 10(5): e1004282.
14. Jackson DA, Pombo A (1998) Replicon clusters are stable units of chromosome structure: Evidence that nuclear organization contributes to the efficient activation and propagation of S phase in human cells. *J Cell Biol* 140(6):1285–1295.
15. Conti C, et al. (2007) Replication fork velocities at adjacent replication origins are coordinately modified during DNA replication in human cells. *Mol Biol Cell* 18(8): 3059–3067.
16. Blow JJ, Ge XQ (2009) A model for DNA replication showing how dormant origins safeguard against replication fork failure. *EMBO Rep* 10(4):406–412.
17. Kunnev D, et al. (2015) Effect of minichromosome maintenance protein 2 deficiency on the locations of DNA replication origins. *Genome Res* 25(4):558–569.
18. Lukas C, et al. (2011) 53BP1 nuclear bodies form around DNA lesions generated by mitotic transmission of chromosomes under replication stress. *Nat Cell Biol* 13(3): 243–253.
19. Naim V, Wilhelm T, Debatisse M, Rosselli F (2013) ERCC1 and MUS81-EME1 promote sister chromatid separation by processing late replication intermediates at common fragile sites during mitosis. *Nat Cell Biol* 15(8):1008–1015.
20. Minocherhomji S, et al. (2015) Replication stress activates DNA repair synthesis in mitosis. *Nature* 528(7581):286–290.
21. Ying S, et al. (2013) MUS81 promotes common fragile site expression. *Nat Cell Biol* 15(8):1001–1007.
22. Harrigan JA, et al. (2011) Replication stress induces 53BP1-containing OPT domains in G1 cells. *J Cell Biol* 193(1):97–108.
23. Rappold I, Iwabuchi K, Date T, Chen J (2001) Tumor suppressor p53 binding protein 1 (53BP1) is involved in DNA damage-signaling pathways. *J Cell Biol* 153(3):613–620.
24. Anderson L, Henderson C, Adachi Y (2001) Phosphorylation and rapid relocalization of 53BP1 to nuclear foci upon DNA damage. *Mol Cell Biol* 21(5):1719–1729.
25. Polo SE, Jackson SP (2011) Dynamics of DNA damage response proteins at DNA breaks: a focus on protein modifications. *Genes Dev* 25(5):409–433.
26. Chan KL, North PS, Hickson ID (2007) BLM is required for faithful chromosome segregation and its localization defines a class of ultrafine anaphase bridges. *EMBO J* 26(14):3397–3409.
27. Chan KL, Hickson ID (2009) On the origins of ultra-fine anaphase bridges. *Cell Cycle* 8(19):3065–3066.
28. Barefield C, Karlseder J (2012) The BLM helicase contributes to telomere maintenance through processing of late-replicating intermediate structures. *Nucleic Acids Res* 40(15):7358–7367.
29. Biebricher A, et al. (2013) PICH: A DNA translocase specially adapted for processing anaphase bridge DNA. *Mol Cell* 51(5):691–701.
30. Bunting SF, et al. (2010) 53BP1 inhibits homologous recombination in Brca1-deficient cells by blocking resection of DNA breaks. *Cell* 141(2):243–254.
31. Petrakis TG, et al. (2016) Exploring and exploiting the systemic effects of deregulated replication licensing. *Semin Cancer Biol* 37-38:3–15.
32. O'Keefe RT, Henderson SC, Spector DL (1992) Dynamic organization of DNA replication in mammalian cell nuclei: Spatially and temporally defined replication of chromosome-specific alpha-satellite DNA sequences. *J Cell Biol* 116(5):1095–1110.
33. Morgan M, et al. (2009) ShortRead: A bioconductor package for input, quality assessment and exploration of high-throughput sequence data. *Bioinformatics* 25(19): 2607–2608.
34. Liao Y, Smyth GK, Shi W (2013) The Subread aligner: Fast, accurate and scalable read mapping by seed-and-vote. *Nucleic Acids Res* 41(10):e108.
35. Weddington N, et al. (2008) ReplicationDomain: A visualization tool and comparative database for genome-wide replication timing data. *BMC Bioinformatics* 9:530.